










## Improved Carbon and Nitrogen Isotopic Ratios for CH<sub>3</sub>CN in Titan's Atmosphere Using ALMA

JONATHON NOSOWITZ <sup>1,2</sup> MARTIN A. CORDINER <sup>2,1</sup> CONOR A. NIXON <sup>2</sup> ALEXANDER E. THELEN <sup>3</sup>  
ZBIGNIEW KISIEL <sup>4</sup> NICHOLAS A. TEANBY <sup>5</sup> PATRICK G. J. IRWIN <sup>6</sup> STEVEN B. CHARNLEY <sup>2</sup> AND  
VÉRONIQUE VUITTON <sup>7</sup>

<sup>1</sup>*Department of Physics, The Catholic University of America, Washington, DC 20064, USA*

<sup>2</sup>*Solar System Exploration Division, NASA Goddard Space Flight Center, Greenbelt, MD 20771, USA*

<sup>3</sup>*Division of Geological and Planetary Sciences, California Institute of Technology, Pasadena, CA 91125, USA*

<sup>4</sup>*Institute of Physics, Polish Academy of Sciences, Al. Lotników 32/46, 02-668 Warszawa, Poland*

<sup>5</sup>*School of Earth Sciences, University of Bristol, Bristol BS8 1RJ, UK*

<sup>6</sup>*Atmospheric, Oceanic and Planetary Physics, Clarendon Laboratory, University of Oxford, Oxford OX1 3PU, UK*

<sup>7</sup>*Univ. Grenoble Alpes, CNRS, IPAG, 38000 Grenoble, France*

(Accepted PSJ, March 2025)

### ABSTRACT

Titan, Saturn's largest satellite, maintains an atmosphere composed primarily of nitrogen (N<sub>2</sub>) and methane (CH<sub>4</sub>) that leads to a complex organic chemistry. Some of the nitriles (CN-bearing organics) on Titan are known to have substantially enhanced <sup>15</sup>N abundances compared to Earth and to Titan's dominant nitrogen (N<sub>2</sub>) reservoir. The <sup>14</sup>N/<sup>15</sup>N isotopic ratio in Titan's nitriles can provide better constraints on the synthesis of nitrogen-bearing organics in planetary atmospheres as well as insights into the origin of Titan's large nitrogen abundance. Using high signal-to-noise ratio (> 13), disk-integrated observations obtained with the Atacama Large Millimeter/submillimeter Array (ALMA) Band 6 receiver (211-275 GHz), we measure the <sup>14</sup>N/<sup>15</sup>N and <sup>12</sup>C/<sup>13</sup>C isotopic ratios of acetonitrile (CH<sub>3</sub>CN) in Titan's stratosphere. Using the Nonlinear optimal Estimator for Multivariate spectral analysis (NEMESIS), we derived the CH<sub>3</sub>CN/<sup>13</sup>CH<sub>3</sub>CN ratio to be 89.2 ± 7.0 and the CH<sub>3</sub>CN/CH<sub>3</sub><sup>13</sup>CN ratio to be 91.2 ± 6.0, in agreement with the <sup>12</sup>C/<sup>13</sup>C ratio in Titan's methane, and other Solar System species. We found the <sup>14</sup>N/<sup>15</sup>N isotopic ratio to be 68.9 ± 4.2, consistent with previously derived values for HCN and HC<sub>3</sub>N, confirming an enhanced <sup>15</sup>N abundance in Titan's nitriles compared with the bulk atmospheric N<sub>2</sub> value of <sup>14</sup>N/<sup>15</sup>N = 168, in agreement with chemical models incorporating isotope-selective photodissociation of N<sub>2</sub> at high altitudes.

*Keywords:* Titan — Remote Sensing — Radio/sub-mm interferometry — Atmospheric Chemistry

### 1. INTRODUCTION

The origin and evolution of the atmosphere of Titan, Saturn's largest satellite, has been an area of interest for many years. Titan's atmosphere is substantial, with intricate chemistry for a moon, and can provide a template for understanding the compositions of primitive carbon/nitrogen-dominated (exo-)planetary atmospheres. As we continue to investigate Titan's atmosphere, more questions arise on topics such as cloud and

haze formation, chemical pathways, interactions with surface and sub-surface features, and the full extent of Titan's organic inventory (Nixon et al. 2018; MacKenzie et al. 2021). Titan possesses a thick atmosphere composed primarily of molecular nitrogen (N<sub>2</sub>) at about 98% and methane (CH<sub>4</sub>) at about 2% in the stratosphere, but the origins of these surprisingly abundant gases are not well known. Titan's methane was first observed by Kuiper (1944), and various ideas have been put forward to explain its presence and persistence (Nixon et al. 2012), such as diffusion from subsurface reservoirs (Kossacki & Lorenz 1996), episodic outgassing from clathrate

hydrates (Tobie et al. 2006; Choukroun et al. 2010), or release from cryo-lava flows (Davies et al. 2016).

Glein (2015) suggested that the gases responsible for forming Titan’s dense, nitrogen-rich atmosphere were originally trapped in its core, and that subsequent hydrothermal and cryovolcanic processes were critical to the formation of Titan’s atmosphere. However, this is reliant on chemical reactions, outgassing, and transport mechanisms to produce the gas abundances currently observed. Glein (2015) showed that this method is plausible through mass balance and chemical equilibrium calculations, but also acknowledged that missing information, such as a value for a reasonable outgassing efficiency, makes it challenging to conclusively validate the theory. Thus, an external (cometary) source of Titan’s nitrogen may be plausible. The isotopic ratios derived for cometary gases are similar to those of Titan’s atmosphere, suggesting that the primordial  $\text{NH}_3$  reservoir represented by cometary ices could be the source of Titan’s nitrogen (Mandt et al. 2014).

The  $\text{N}_2$  and  $\text{CH}_4$  in Titan’s atmosphere form the basis of a complex chemical reaction network, yet the chemistry involving nitrogen is still not fully constrained (Hörst 2017; Nixon 2024). It is particularly important to understand the chemistry of nitriles, as they are the most abundant nitrogen-containing photochemical products and may play a role in prebiotic syntheses (Oro et al. 1990), in addition to their importance in the organic chemistry of space, and the potential for life beyond Earth in general.

Nitriles often possess a large dipole moment, and thus their rotational transitions can be detected in Titan’s atmosphere at mm/sub-mm wavelengths, including  $\text{HCN}$ ,  $\text{HC}_3\text{N}$ ,  $\text{CH}_3\text{C}_3\text{N}$ ,  $\text{C}_2\text{H}_5\text{CN}$  and more (Hörst 2017; Cordiner et al. 2015; Palmer et al. 2017; Thelen et al. 2020; Marten et al. 2002; Rengel et al. 2011, 2022). These molecules, and a diverse population of other organics, are generated in Titan’s upper atmosphere through high-altitude photochemistry, following dissociation by UV photons, and collisions with charged particles from Saturn’s magnetosphere, and/or galactic cosmic rays.

Previously developed photochemical models (*e.g.* Dobrijevic & Loison 2018; Vuitton et al. 2019; Wilson & Atreya 2004; Willacy et al. 2016) obtain a moderately good agreement with the observed abundances of many nitrogen-bearing species in Titan’s atmosphere, suggesting good progress in our quantitative understanding of the relevant chemical processes. However, there still exist significant gaps in our knowledge of Titan’s photochemistry, in terms of the detailed reaction pathways as a function of altitude. The available photochemical

models make different assumptions regarding the relevant reaction pathways, and the  $^{14}\text{N}/^{15}\text{N}$  ratios in Titan’s nitriles are particularly sensitive to some of these assumptions. Enrichment (or isotopic fractionation) of  $^{15}\text{N}$  relative to Titan’s bulk  $\text{N}_2$  reservoir is theorized to occur as a result of isotope selective photodissociation of  $\text{N}_2$  (Liang et al. 2007), which involves the more efficient self-shielding of  $^{14}\text{N}_2$  compared with the less abundant  $^{14}\text{N}^{15}\text{N}$  isotopologue at high altitudes, leading to a reservoir of gas-phase atomic nitrogen that is isotopically enriched in  $^{15}\text{N}$ . The resulting  $^{15}\text{N}$  enrichment is readily passed on to nitrogen-bearing photochemical products. However, the atomic  $^{14}\text{N}/^{15}\text{N}$  ratio is observationally unconstrained, and is sensitive to the various model parameters. Incorporation of  $^{15}\text{N}$  into nitriles occurs at different rates depending on the altitude-dependent reaction pathways; indeed, the  $^{14}\text{N}/^{15}\text{N}$  isotopic ratio in  $\text{CH}_3\text{CN}$  has been shown to depend on the relative efficiencies of the different formation pathways (Dobrijevic & Loison 2018), which are not yet fully constrained by experiments. Further studies of the  $^{14}\text{N}/^{15}\text{N}$  ratios in Titan’s nitriles are therefore needed, to improve our understanding of the relevant chemical processes, which will lead to a better understanding of nitrogen chemistry (including isotope chemistry) in planetary atmospheres.

The first  $^{14}\text{N}/^{15}\text{N}$  isotopic ratio measurement of Titan’s atmosphere was by Marten et al. (2002), who used the Institut de Radioastronomie Millimétrique (IRAM) 30-m telescope to derive a value of  $\text{HC}^{14}\text{N}/\text{HC}^{15}\text{N} = 60\text{--}70$  in the stratosphere. This was followed by Gurwell (2004) using the Submillimeter Array, who obtained  $94 \pm 13$  and  $72 \pm 9$  depending on the assumed temperature profile. Vinatier et al. (2007) subsequently derived  $\text{HC}^{14}\text{N}/\text{HCN}^{15}\text{N} = 56 \pm 8$  using Cassini infrared spectroscopy. Courtin et al. (2011) used the Spectral and Photometric Imaging Receiver (SPIRE) instrument on the Herschel spacecraft to derive a ratio of  $76 \pm 6$ . The  $\text{HC}^{14}\text{N}/\text{HC}^{15}\text{N}$  ratio was further refined by Molter et al. (2016) who obtained  $72.2 \pm 2.2$  using high spectral-resolution ALMA observations. Using in-situ mass spectrometry, Cassini-Huygens measured the atmospheric  $^{14}\text{N}_2/^{15}\text{N}^{14}\text{N}$  ratio, from which a  $^{14}\text{N}/^{15}\text{N}$  ratio of  $167.7 \pm 0.6$  was derived in  $\text{N}_2$ , which represents the dominant atmospheric nitrogen reservoir (Niemann et al. 2010).

More recently, Cordiner et al. (2018) used ALMA to obtain a  $^{14}\text{N}/^{15}\text{N}$  ratio of  $67 \pm 14$  in  $\text{HC}_3\text{N}$ , while Palmer et al. (2017), and Iino et al. (2020) measured  $\text{CH}_3\text{C}^{14}\text{N}/\text{CH}_3\text{C}^{15}\text{N}$  ratios of  $89 \pm 5$ , and  $125_{-44}^{+145}$ , respectively. While there is some apparent scatter among the various measurements, a significant difference is evident between the  $^{15}\text{N}$  fractions in the (trace) photo-

chemical products and the (bulk) nitrogen ( $N_2$ ) reservoir, which can be explained as a result of isotope selective  $N_2$  photodissociation by solar radiation (Liang et al. 2007; Vuitton et al. 2019). The significance of any differences in the degree of  $^{15}N$  enrichment among different nitriles is yet to be investigated in detail. As one of the most abundant nitriles in Titan’s atmosphere, more accurate measurements of the  $CH_3CN$  isotopologues, in particular, are justified, to help test and improve models for Titan’s nitrogen chemistry.

## 2. OBSERVATIONS

To investigate Titan’s high-altitude nitrogen chemistry, we obtained observations using the Atacama Large Millimeter/submillimeter Array (ALMA) Band 6 receiver (211-275 GHz;  $\sim 1.1$ -1.4 mm), in 2019 as part of project #2019.1.00783.S. Three spectral settings were observed (see Thelen et al. (2020) for details), the first of which (Science Goal 1; SG1) covered the CO  $J = 2 - 1$  line, and the remaining two (SGs 2 and 3) covered observations of multiple nitrile species and their carbon and nitrogen isotopes. The data from SGs 2 and 3 used in the present study were observed in several non-consecutive frequency intervals between 256.9–257.8 GHz and 267.0–268.9 GHz (see Table 1).

As described by Thelen et al. (2020), the data were taken during multiple execution blocks between November 14 and December 16, 2019 using ALMA configurations C43-1, C43-2 (maximum baselines ranging from 160 to 314 m), and C43-3 (maximum baselines of 500 m). The resulting beam size was  $1.54'' \times 1.14''$  in the 256-257 GHz range and  $1.56'' \times 1.11''$  in the 267-268 GHz range, so Titan ( $\approx 1.0''$  diameter on the sky, including its solid disk and extended atmosphere) was not resolved, enabling the maximum sensitivity per beam for disk-averaged studies of Titan’s entire Earth-facing atmosphere. The spectral resolution of the  $CH_3CN$  and  $CH_3^{13}CN$  isotopologues was 488 kHz and the resolution for the  $^{13}CH_3CN$  and  $CH_3C^{15}N$  isotopologues was 976 kHz. The data were processed and calibrated using version 5.6.1-8 of the Common Astronomy Software Applications (CASA) pipeline using standard scripts provided by the Joint ALMA Observatory (JAO). Additional bandpass calibration smoothing was performed, to improve the spectral noise per channel, and the `tclean` procedure was used to reconstruct the sky model. For a more complete description of the observations and data processing, we refer the reader to Thelen et al. (2020).

A list of the observed  $CH_3CN$  spectral lines of relevance to the present study, their frequencies and upper state energies ( $E_u$ ) are shown in Table 1. The total

signal-to-noise ratios (SNRs) integrated across the full-width of all detected  $CH_3CN$  lines are: 1450 for the major isotopologue, 13 for  $^{13}CH_3CN$ , 15 for  $CH_3^{13}CN$  and 16 for  $CH_3C^{15}N$ .

## 3. RADIATIVE TRANSFER MODELING

From the processed data cubes, disk-averaged spectra were extracted using a circular aperture with a radius of  $1.8''$ , which includes Titan up to the top of its atmosphere plus half a beam to account for all emission. Titan’s disk was divided into 35 annuli corresponding to different emission angles from 3-75 degrees covering the center of Titan up to a tangential altitude of 1200 km (Teanby et al. 2013); the vertical extent of our model. Spectral models were generated using the line-by-line module of the Nonlinear optimal Estimator for Multi-variatiE spectral analySIS (NEMESIS) radiative transfer and retrieval tool (Irwin et al. 2008). NEMESIS applies an iterative minimization technique to the cost function (including the goodness of fit,  $\chi^2$ , combined with the a-priori errors) in order to obtain an optimized spectral model, temperature, and abundance profiles as a function of altitude. NEMESIS includes the necessary physical parameters such as spontaneous emission and absorption of radiation, on and off-limb emission angles, continuum opacity and thermal and pressure broadening, as well as temperature dependence when computing model fluxes as a function of wavelength. This allows a full characterization of the observed spectral line profiles, leading to robust abundance measurements.

To further improve the accuracy of our model retrieval results, updates were made to the spectral line database and instrumental broadening function. The NEMESIS line database was updated to the GEISA 211 format (Jacquinet-Husson et al. 2005) for additional precision on the rest frequencies and intensities. We initially used the line data from The Cologne Database for Molecular Spectroscopy (CDMS) (Müller et al. 2001) but found discrepancies in the line intensities and partition function coefficients for the major isotopologue and  $^{13}C$  minor isotopologues. These values were not sufficiently accurate in this frequency range and therefore, all of the values were re-computed without hyperfine or vibrational corrections in a self-consistent manner. Note that the hyperfine splittings for all relevant transitions are much smaller than the resolution of our observed spectra. We refer the reader to Appendix A for more details. The partition functions for all of the isotopologues were tabulated for inclusion in NEMESIS using a third order polynomial fit to the re-computed values listed in Table 2. We also updated the instrumental line shape used by NEMESIS, to account for the intrinsic (non-Gaussian)

**Table 1.** Observed CH<sub>3</sub>CN isotopologue transitions

Species	Transition <sup>a</sup>	Rest. Freq. (GHz)	$E_u$ (K)
CH <sub>3</sub> CN	14 <sub>6</sub> -13 <sub>6</sub>	257.3491793	349.7
CH <sub>3</sub> CN	14 <sub>5</sub> -13 <sub>5</sub>	257.4035843	271.2
CH <sub>3</sub> CN	14 <sub>4</sub> -13 <sub>4</sub>	257.4481277	206.9
CH <sub>3</sub> CN	14 <sub>3</sub> -13 <sub>3</sub>	257.4827915	156.9
CH <sub>3</sub> CN	14 <sub>2</sub> -13 <sub>2</sub>	257.5075614	121.2
CH <sub>3</sub> CN	14 <sub>1</sub> -13 <sub>1</sub>	257.5224275	99.8
CH <sub>3</sub> CN	14 <sub>0</sub> -13 <sub>0</sub>	257.5273835	92.7
CH <sub>3</sub> <sup>13</sup> CN	14 <sub>3</sub> -13 <sub>3</sub>	257.3555752	156.9
CH <sub>3</sub> <sup>13</sup> CN	14 <sub>2</sub> -13 <sub>2</sub>	257.3802430	121.2
CH <sub>3</sub> <sup>13</sup> CN	14 <sub>1</sub> -13 <sub>1</sub>	257.3950476	99.8
CH <sub>3</sub> <sup>13</sup> CN	14 <sub>0</sub> -13 <sub>0</sub>	257.3999832	92.6
CH <sub>3</sub> C <sup>15</sup> N	15 <sub>5</sub> -14 <sub>5</sub>	267.4868839	281.6
CH <sub>3</sub> C <sup>15</sup> N	15 <sub>4</sub> -14 <sub>4</sub>	267.5323198	217.2
CH <sub>3</sub> C <sup>15</sup> N	15 <sub>3</sub> -14 <sub>3</sub>	267.5676777	167.1
CH <sub>3</sub> C <sup>15</sup> N	15 <sub>2</sub> -14 <sub>2</sub>	267.5929435	131.3
CH <sub>3</sub> C <sup>15</sup> N	15 <sub>1</sub> -14 <sub>1</sub>	267.6081070	109.9
CH <sub>3</sub> C <sup>15</sup> N	15 <sub>0</sub> -14 <sub>0</sub>	267.6131621	102.7
<sup>13</sup> CH <sub>3</sub> CN	15 <sub>5</sub> -14 <sub>5</sub>	267.8245852	281.7
<sup>13</sup> CH <sub>3</sub> CN	15 <sub>4</sub> -14 <sub>4</sub>	267.8698337	217.3
<sup>13</sup> CH <sub>3</sub> CN	15 <sub>3</sub> -14 <sub>3</sub>	267.9050464	167.2
<sup>13</sup> CH <sub>3</sub> CN	15 <sub>2</sub> -14 <sub>2</sub>	267.9302086	131.5
<sup>13</sup> CH <sub>3</sub> CN	15 <sub>1</sub> -14 <sub>1</sub>	267.9453102	110.0
<sup>13</sup> CH <sub>3</sub> CN	15 <sub>0</sub> -14 <sub>0</sub>	267.9503447	102.8

<sup>a</sup> Rotational transitions are denoted as  $J'_{K'} - J''_{K''}$ , where the transition is from the upper state to the lower state and K represents the angular momentum quantum number

shape of the ALMA line spread function, as well as including the potential effects of Doppler broadening of the lines due to Titan’s zonal winds (see Appendix B for details).

Optimization of the vertical abundance profile began with a reasonable guess based on prior measurements. For the major CH<sub>3</sub>CN isotopologue, we used an a priori profile based on the disk-averaged measurements from Marten et al. (2002) up to 500 km, supplemented by data from the model of Loison et al. (2015) up to 1200 km. The error on this ‘a-priori’ profile was set to a constant value of 100%. From the N<sub>2</sub> broadening parameters of CH<sub>3</sub>CN calculated by Dudaryonok et al. (2015), we assumed an average value for the Lorentzian half-width using the  $K = 0$  &  $K = 5$ ,  $J = 14 - 13$  coefficients ( $\Gamma = 0.158 \text{ cm}^{-1} \text{ atm}^{-1}$ ) and temperature exponent ( $\alpha = 0.60$ ). The collision-induced absorption (CIA) parameters used include all combinations of N<sub>2</sub>, CH<sub>4</sub>, and H<sub>2</sub> and are calculated by following the routines of Borysow & Frommhold (1986a,b,c, 1987) and

Borysow & Tang (1993). The atmospheric temperature vertical profile was obtained by modeling the ALMA CO data obtained contemporaneously with our observations (see Thelen et al. (2020) for details).

A correlation length of 3.0 atmospheric scale heights was used to internally smooth the optimized vertical profiles. The observed ALMA flux spectra were scaled by a constant factor ( $\approx 1.02$ ) to produce a match between the modeled and observed continuum levels. This scaling mitigates errors on the ALMA flux scale (which may be as much as  $\approx 10\%$ , due to uncertainty in the amplitude calibrator flux), as well as accounting for small errors in the assumed (a priori) temperature around the tropopause, which determines the model continuum level. The CH<sub>3</sub>CN major isotopologue profile was continuously retrieved at each altitude to obtain an optimized fit to the observed spectral line profiles. The retrieved profile was found to be consistent across several forms of a priori profiles (see Appendix E) as shown in Figure 9.

The minor CH<sub>3</sub>CN isotopologue spectra are noisier and contain less vertical information than the major isotopologue, so we used the best-fitting CH<sub>3</sub>CN main isotopologue abundance profile scaled by a uniform factor, which was varied to obtain the best fit for those species. The results of an attempted, continuously-variable CH<sub>3</sub>C<sup>15</sup>N retrieval, are discussed in Appendix C.

Finally, we tested the sensitivity of our retrieved isotopic ratios to uncertainties in the atmospheric temperature profile (Thelen et al. 2020), which vary between 1–5 K as a function of altitude. Due to the close similarities in the observed frequencies and energy levels of the different isotopologues, their line strengths scale similarly with temperature, so these uncertainties amount only to an additional error of  $< 0.8\%$  on the retrieved isotopic ratios.

## 4. RESULTS

Our CH<sub>3</sub>CN spectral fits and retrieved vertical abundance and temperature profiles are shown in Figure 1. We derived scaling factors representative of the mean isotopic ratios over Titan’s disk-averaged atmosphere, for the three minor CH<sub>3</sub>CN isotopologues, including the <sup>15</sup>N isotopologue and both <sup>13</sup>C isotopologues. The CH<sub>3</sub>CN/CH<sub>3</sub>C<sup>15</sup>N isotopic ratio was derived to be  $68.9 \pm 4.2$ , the CH<sub>3</sub>CN/<sup>13</sup>CH<sub>3</sub>CN ratio was derived to be  $89.2 \pm 7.0$ , and the CH<sub>3</sub>CN/CH<sub>3</sub><sup>13</sup>CN ratio was derived to be  $91.2 \pm 6.0$ . Our derived <sup>14</sup>N/<sup>15</sup>N isotopic ratio for the major isotopologue is shown for comparison with previously obtained ratios for HCN, HC<sub>3</sub>N and CH<sub>3</sub>CN as well as N<sub>2</sub> in Figure 2.

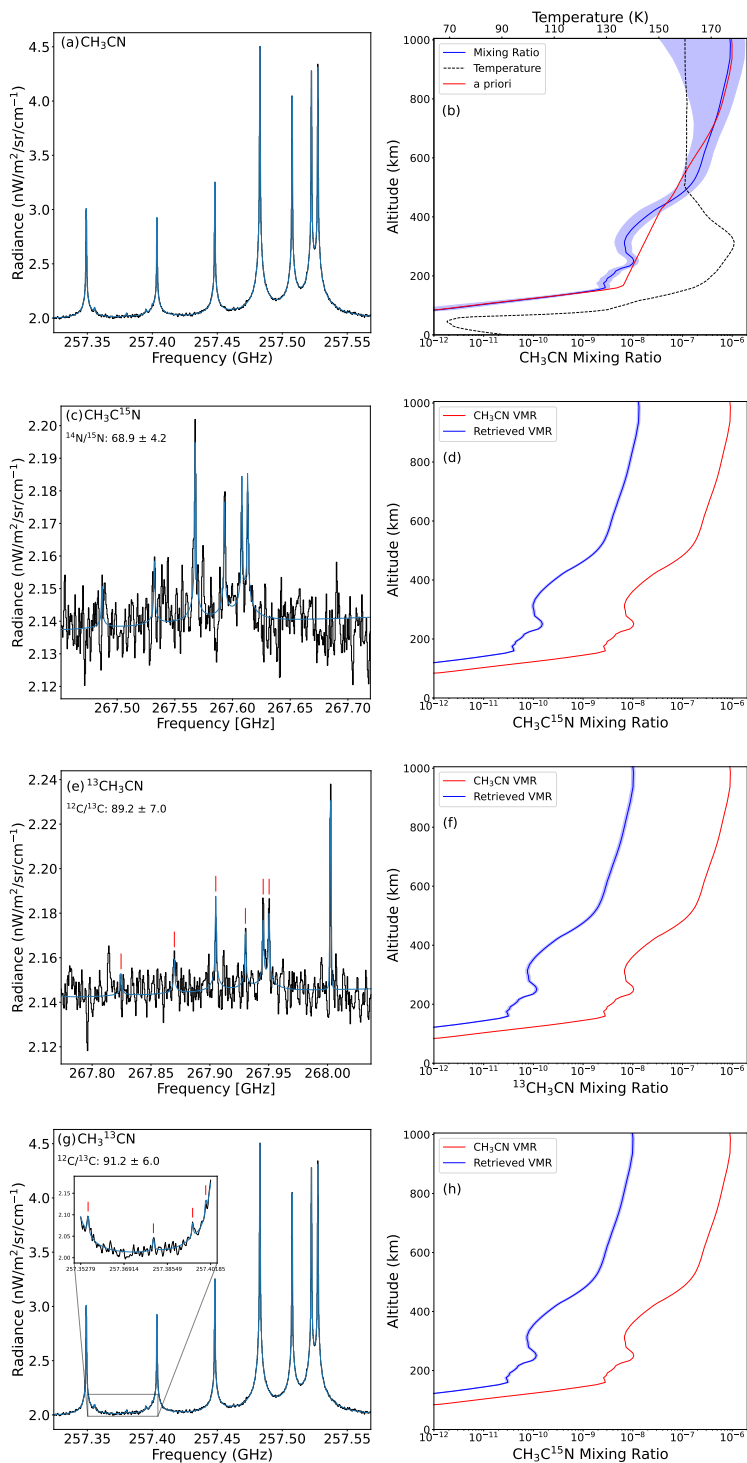


**Figure 1.** Optimized model fits for all isotopologues in the left column, panels (a), (c), (e), and (g). The data is in black and the model is in blue. The molecule is identified in the top left corner of the panel along with the corresponding scaling factor. The respective retrieved vertical profiles (volume mixing ratios or VMRs) are in the right column, panels (b), (d), (f), and (h). In all profiles, the red line is the a priori profile, the blue line is the retrieved VMR profile and the shaded region is the error on the retrieved VMR profile. For the major isotopologue, the dashed black line in panel (b) is the temperature profile. The error envelope of the minor isotopologues is quite narrow, it is within 6-8% of the obtained isotope ratio value. The red ticks in (e) and (g) identify the  $^{13}\text{CH}_3\text{CN}$  and  $\text{CH}_3^{13}\text{CN}$  lines, respectively, in the data. The highest frequency line in (e) is the  $J = 30 - 29$ ,  $K_a = 3$  transition of  $\text{C}_2\text{H}_5\text{CN}$  (propionitrile; ethyl cyanide) at 268.0025 GHz.



Within the noise, our spectral models provide an excellent fit to the observed Titan continuum, line cores and line wings. In the lower stratosphere (below 150 km altitude), our retrieved  $\text{CH}_3\text{CN}$  vertical abundance (VMR) profile matches closely the steepness of the Marten et al. (2002) a-priori. Our retrieved abundances drop somewhat below the a-priori in the mid-to-upper stratosphere, with the notable exception of a maximum around 250 km, although there may be some doubt as to the physical origin of this relatively narrow feature, since it is not present in the ALMA profile retrieved by Lellouch et al. (2019), or the photochemical model results of Vuitton et al. (2019) and Dobrijevic & Loison (2018). Considering our observations are averaged over Titan’s entire Earth-facing hemisphere, the resulting spectra represent a weighted average across all latitudes and altitudes. It therefore cannot be determined where exactly (latitudinally) in Titan’s atmosphere this peak originates. On the other hand, this feature is found to be necessary to obtain a good fit to the observed spectra — otherwise, the line core and wing strengths cannot be simultaneously reproduced.

Based on the  $\text{CH}_3\text{CN}$  maps previously published by Thelen et al. (2019, 2024) and Cordiner et al. (2019),  $\text{CH}_3\text{CN}$  is most concentrated around Titan’s poles. The stratospheric  $\text{CH}_3\text{CN}$  enhancement could be consistent with the presence of unresolved abundance peak(s) within the beam, associated with one or both of these regions. It can be speculated that the contribution is potentially coming from the trapping of molecules and subsidence in the (cold) polar regions, possibly at different altitudes around the north and south poles (see Teanby et al. (2008, 2017, 2019), for example).

We then used the contribution functions from our best-fitting radiative transfer models to calculate weighted mean emission altitudes, which represent the average altitude to which our results are sensitive. These were determined to be  $\sim 230$  km for  $^{13}\text{CH}_3\text{CN}$  and  $\text{CH}_3\text{C}^{15}\text{N}$  (and  $\sim 246$  km for the major isotopologue).

To make a detailed comparison with the  $\text{CH}_3\text{CN}/\text{CH}_3\text{C}^{15}\text{N}$  vertical profiles produced by photochemical models, we also performed a continuously-variable  $\text{CH}_3\text{C}^{15}\text{N}$  VMR fit. However, the spectroscopic signal-to-noise ratio of 16 was found to be insufficient to provide useful constraints on the  $^{14}\text{N}/^{15}\text{N}$  ratio as a function of altitude (see Appendix C).

## 5. DISCUSSION

We now compare our isotopic ratios to those previously obtained in the Titan literature. We find that our  $\text{CH}_3\text{CN}/\text{CH}_3\text{C}^{15}\text{N}$  ratio of  $68.9 \pm 4.2$  is significantly lower than the  $^{14}\text{N}/^{15}\text{N}$  ratio in  $\text{N}_2$  of  $167.7 \pm$

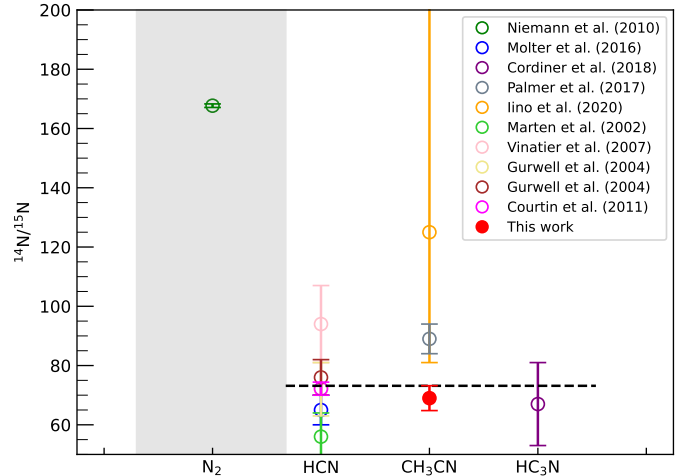


**Figure 2.** Previously derived  $^{14}\text{N}/^{15}\text{N}$  isotopic ratios for molecules in Titan’s atmosphere, including the value derived in this work in red. The  $\text{N}_2$  data point is plotted against a gray background to distinguish it as the main atmospheric nitrogen reservoir. The black dashed line is the error weighted average of previously-measured  $^{14}\text{N}/^{15}\text{N}$  ratios from Iino et al. (2020), Marten et al. (2002), Vinatier et al. (2007), Gurwell (2004), Courtin et al. (2011), Molter et al. (2016) and Cordiner et al. (2018).

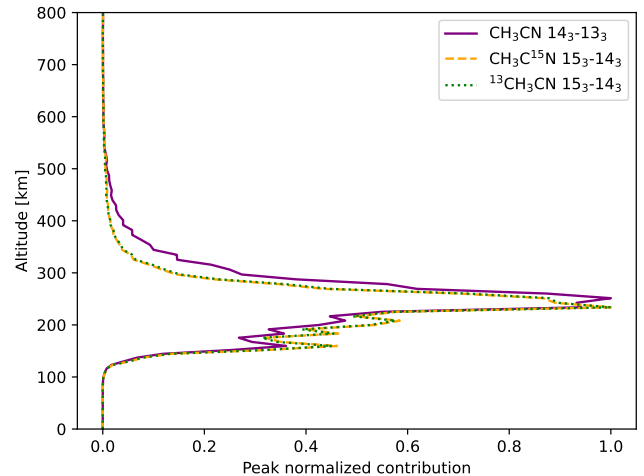


**Figure 3.** Contribution functions for the strongest lines ( $K=3$ ) of  $\text{CH}_3\text{CN}$  and its minor isotopologues.

0.6 obtained by Cassini mass spectrometry (Niemann et al. 2010), indicating strong  $^{15}\text{N}$  enrichment in Titan’s  $\text{CH}_3\text{CN}$ . On the other hand, our result is within  $1.6\text{-}\sigma$  of the previous Cassini CIRS measurement for  $\text{HCN}$  ( $56 \pm 8$ ; Vinatier et al. 2007). Additionally, our ratio is within  $1\text{-}\sigma$  of the Marten et al. (2002)  $\text{HCN}$  value of 60–70, about  $2\text{-}\sigma$  of both derived  $^{14}\text{N}/^{15}\text{N}$  ratios in  $\text{HCN}$  of  $94 \pm 13$  and  $108 \pm 20$  from Gurwell (2004), and is within  $1.2\text{-}\sigma$  of the Courtin et al. (2011) ratio of  $76 \pm$

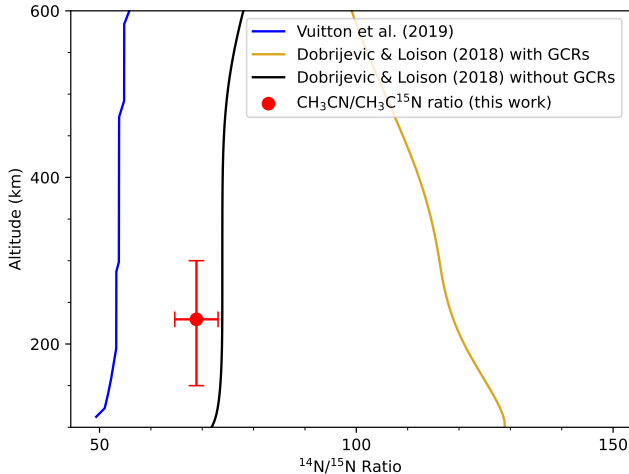


**Figure 4.**  $\text{CH}_3\text{CN}/\text{CH}_3\text{C}^{15}\text{N}$  isotopic ratio (red point) derived from our scale-factor retrieval, with horizontal error bars showing the error on the ratio value and the vertical bar spanning the region of highest sensitivity: 150-300 km. For comparison, the chemical model results of Vuitton et al. (2019) (blue line) and Dobrijevic & Loison (2018) (black, without cosmic rays and gold, with cosmic rays), are shown.

6. The HCN measurement using ALMA of  $72.2 \pm 2.2$  by Molter et al. (2016) is also within  $1\text{-}\sigma$  of our derived ratio. Within the errors, our result is also consistent with the  $^{14}\text{N}/^{15}\text{N}$  ratio in  $\text{HC}_3\text{N}$  ( $67 \pm 14$ ; Cordiner et al. 2018), and within  $1.3\text{-}\sigma$  of the previous best value for the  $\text{CH}_3\text{CN}/\text{CH}_3\text{C}^{15}\text{N}$  ratio of  $125^{+145}_{-44}$ , obtained using ALMA archival flux calibration data by Iino et al. (2020). Although the apparent difference between our value and that of Iino et al. (2020) could be explained solely as a result of statistical noise, it should be noted that our improved values for the spectral line intensities and partition functions compared with those in the CDMS database (see Appendix A) resulted in a downward revision of the  $^{14}\text{N}/^{15}\text{N}$  ratio by  $\sim 18\%$ ,  $\sim 23\%$  for  $^{12}\text{C}/^{13}\text{C}$  and  $\sim 34\%$  for  $\text{CH}_3\text{CN}/\text{CH}_3^{13}\text{CN}$ , so this could explain some of the discrepancy.

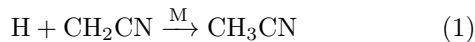
Overall, our derived ratio is in relatively good agreement with the previously obtained nitrogen isotopic ratios, with the exception of  $\text{N}_2$ . By far the dominant form of nitrogen in Titan’s atmosphere is  $\text{N}_2$ , so we take the  $^{14}\text{N}/^{15}\text{N}$  ratio in  $\text{N}_2$  to be representative of Titan’s intrinsic isotopic composition. Isotope-selective photodissociation of  $\text{N}_2$  in the upper atmosphere provides a reservoir of  $^{15}\text{N}$ -enriched atomic nitrogen that feeds into the altitude dependent nitrogen chemistry, resulting in the synthesis of  $^{15}\text{N}$ -enriched nitriles such as  $\text{CH}_3\text{CN}$ . In Figure 57 of Vuitton et al. (2019), the peak density for atomic  $^{14}\text{N}$  and  $^{15}\text{N}$  occurs in Titan’s thermosphere between 1100-1200 km, falling rapidly below

$\sim 700$  km. However, the atomic  $^{14}\text{N}/^{15}\text{N}$  isotopic ratio reaches a peak value of  $\sim 25$  at  $\sim 900$  km, below the point of the peak atomic  $^{14}\text{N}$  and  $^{15}\text{N}$  values. There are approximately constant values for the wings of the distribution of the  $^{14}\text{N}/^{15}\text{N}$  ratio:  $\sim 85$  at  $\sim 1200$  km and above and  $\sim 100$  at  $\sim 800$  km and below. Thus, the incorporation of fractionated nitrogen, and therefore production of nitriles, occurs primarily above  $\sim 700$  km in the Vuitton et al. (2019) model, followed by downward mixing and diffusion toward the stratosphere, into the region between 150-300 km, to which our ALMA observations are most sensitive. The enriched  $^{15}\text{N}$  abundance in the main nitrile production thus leads to a decrease in the  $^{14}\text{N}/^{15}\text{N}$  isotopic ratio for  $\text{CH}_3\text{CN}$ . The large difference between the isotopic ratios in  $\text{N}_2$  and  $\text{CH}_3\text{CN}$  is consistent with this picture. Also comparing the  $^{14}\text{N}/^{15}\text{N}$  ratio profiles for HCN,  $\text{CH}_3\text{CN}$  and  $\text{HC}_3\text{N}$  shown in Figure 58 of Vuitton et al. (2019) reveals that they should be expected to follow a similar general trend, with decreased values at altitudes below  $\sim 800$  km.

Isotopic ratios for  $^{12}\text{C}/^{13}\text{C}$  have previously been measured on Titan for  $\text{CH}_4$  (Niemann et al. 2010),  $\text{CH}_3\text{D}$  (Bézar et al. 2007),  $\text{CO}_2$  (Nixon et al. 2008b),  $\text{CO}$  (Serigano et al. 2016; Rengel et al. 2014; Courtin et al. 2011),  $\text{C}_4\text{H}_2$  (Jolly et al. 2010),  $\text{C}_2\text{H}_2$  (Nixon et al. 2008a),  $\text{C}_2\text{H}_6$  (Nixon et al. 2008a),  $\text{HC}_3\text{N}$  (Jennings et al. 2008), and HCN (Molter et al. 2016; Hidayat et al. 1997; Rengel et al. 2014; Courtin et al. 2011). Comparing the error weighted mean isotopic ratio for these molecules,  $89.8 \pm 6.9$ , to our derived  $^{12}\text{C}/^{13}\text{C}$  ratios in  $\text{CH}_3\text{CN}$  of  $89.2 \pm 7.0$  and  $91.2 \pm 6.0$ , we find that they are all consistently within a  $1\text{-}\sigma$  error margin. The observed  $^{12}\text{C}/^{13}\text{C}$  ratios are therefore consistent with the dominant carbon reservoir in Titan’s atmosphere Niemann et al. (2010); Nixon et al. (2012); Mandt et al. (2012) — as expected considering a lack of strong isotopic fractionation mechanisms involving carbon, at the altitudes we observed. Unlike  $\text{N}_2$ ,  $\text{CH}_4$  is not subject to isotope-selective self-shielding, so variable  $^{12}\text{C}/^{13}\text{C}$  ratios among the different  $\text{CH}_3\text{CN}$  carbon atoms (as well as other molecules) are not expected. Additionally, when comparing our derived  $^{12}\text{C}/^{13}\text{C}$  ratios to the error-weighted mean for comets ( $88.6 \pm 6.5$ , which excludes the outlier for  $\text{H}_2\text{CO}$  in comet 67P; Altwegg et al. 2020), and with the terrestrial value of 89.0, we also find that our measurements are within  $1\text{-}\sigma$ . Thus, our  $^{12}\text{C}/^{13}\text{C}$  ratios are in good agreement with the values previously derived for Titan and various other Solar System bodies, including other bodies within the Saturnian system (see Nomura et al. 2022, and references therein). We thus confirm the trend for a lower degree of isotopic fraction-

ation in carbon than for nitrogen, across various Solar System bodies.

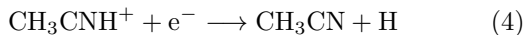
The improved accuracy of our  $\text{CH}_3\text{CN}/\text{CH}_3\text{C}^{15}\text{N}$  ratio compared with [Iino et al. \(2020\)](#) leads to new constraints on models for the  $\text{CH}_3\text{CN}$  production pathways and nitrogen fractionation processes in Titan’s atmosphere. The model by [Vuitton et al. \(2019\)](#) includes multiple pathways to  $\text{CH}_3\text{CN}$ , the most important being



and



followed by



[Balucani et al. \(2012\)](#) showed that equation 2, is inefficient since it favors the alternative isomeric product forms —  $\text{CH}_2\text{NCH}$  and  $c\text{-CH}_2(\text{N})\text{CH}$  — rather than  $\text{CH}_3\text{CN}$ . [Dobrijevic & Loison \(2018\)](#) suggested that equation 1 may not be the dominant route to  $\text{CH}_3\text{CN}$  since it primarily occurs at the higher pressures found in the lower atmosphere.

If reaction 3 (followed by reaction 4) is the primary route to  $\text{CH}_3\text{CN}$  (and therefore  $\text{CH}_3\text{C}^{15}\text{N}$  via  $\text{HC}^{15}\text{NH}^+$ ), then this could help explain the similarity between the observed  $^{14}\text{N}/^{15}\text{N}$  isotopic ratios in  $\text{HCN}$  and  $\text{CH}_3\text{CN}$ .

We now compare our derived scaled nitrogen isotopic ratio with the models of [Vuitton et al. \(2019\)](#) and [Dobrijevic & Loison \(2018\)](#) to gain better insight into how  $^{15}\text{N}$  may be incorporated into  $\text{CH}_3\text{CN}$ . At the value of our peak observed altitudinal sensitivity ( $\approx 230$  km), our value of  $^{14}\text{N}/^{15}\text{N} = 69 \pm 4$  is in better agreement with the [Vuitton et al. \(2019\)](#) model value of  $\sim 55$  than the [Dobrijevic & Loison \(2018\)](#) model value of  $\sim 120$  (with galactic cosmic rays; GCRs included; see Figure 4). On the other hand, our observed  $\text{CH}_3\text{CN}/\text{CH}_3\text{C}^{15}\text{N}$  ratio is a closer match with the [Dobrijevic & Loison \(2018\)](#) model without GCRs included. However, cosmic rays are known to play a significant role in the photochemistry and ionization, primarily of Titan’s lower stratosphere and troposphere [Nixon \(2024\)](#), so it is unclear whether this is a useful comparison. Nevertheless, it may indicate that cosmic ray chemistry should not be considered as a strong factor influencing the stratospheric  $\text{CH}_3\text{CN}/\text{CH}_3\text{C}^{15}\text{N}$  ratio.

The importance of magnetospheric electrons is another difference between the [Vuitton et al. \(2019\)](#) and [Dobrijevic & Loison \(2018\)](#) models. In the [Dobrijevic](#)

[& Loison \(2018\)](#) model, dissociation of  $\text{N}_2$  by magnetospheric electrons provides an additional source of atomic nitrogen not included in the [Vuitton et al. \(2019\)](#) model, particularly important in the upper atmosphere (at altitudes 700-1200 km). Since electron-impact dissociation of  $\text{N}_2$  is not isotope-selective, the resulting additional source of atomic nitrogen in this altitude range has a  $^{14}\text{N}/^{15}\text{N}$  ratio equal to that of  $\text{N}_2$ . This causes the total atomic  $^{14}\text{N}/^{15}\text{N}$  ratio to tend towards larger values, with a corresponding impact on the  $^{14}\text{N}/^{15}\text{N}$  ratio for nitriles produced in this region. The fact that our derived isotopic ratio is greater than that of the [Vuitton et al. \(2019\)](#) model but less than the [Dobrijevic & Loison \(2018\)](#) model (without GCRs), would suggest that magnetospheric electrons could be important as a minor source of atomic  $^{15}\text{N}$ .

While our derived isotopic ratios are in good agreement with previous measurements on Titan ([Hörst 2017](#)), it is of interest to compare with other Solar System bodies. Based on the data collated by [Nomura et al. \(2022\)](#) (and references therein), we identify some general trends for the  $^{12}\text{C}/^{13}\text{C}$  and  $^{14}\text{N}/^{15}\text{N}$  isotopic ratios. The carbon ratios are shown to have only small variations from planet to planet and most of the error bars are fairly well constrained. However, some measurements do have errors too large to constrain the exact variations. Most of the measurements for comets also maintain small variations, with the exception of the value of  $40 \pm 14$  ([Altwegg et al. 2020](#)) for  $\text{H}_2\text{CO}$  in comet 67P, while some have large error bars that are also unable to completely constrain the variations. Meteorites have a larger range of variation. In contrast, the nitrogen isotopic ratios are shown to generally vary amongst the objects in the solar system and may have some smaller variations amongst ratios of the same object depending on the molecule of interest.

Given the results of our study, we can speculate about the origin of Titan’s dense nitrogen reservoir. In future studies, it would be useful to gain more insight into the amount of  $\text{N}_2$  that Titan has lost since it formed; the present-day isotopic ratios of heavy, noble gases would also be useful in this regard. This could help determine if Titan’s  $\text{N}_2$  was formed internally through hydrothermal and cryovolcanic processes and/or if the  $\text{N}_2$  was formed through photochemical reactions involving accreted cometary ices. All the nitriles observed to date show a strong  $^{15}\text{N}$  enrichment. As they mix downward, these nitriles condense into aerosols and precipitate onto the surface, so over time, some of the  $^{15}\text{N}$  is removed from the atmosphere. Therefore, the overall atmospheric  $^{14}\text{N}/^{15}\text{N}$  ratio should increase over time, suggesting that Titan’s atmospheric nitrogen could have



been more  $^{15}\text{N}$  rich in the past — possibly more similar to the value of  $\approx 144$  found in comets (Nomura et al. 2022). To confirm this hypothesis will require continued, high-accuracy studies of  $^{14}\text{N}/^{15}\text{N}$  ratios in cometary nitrogen-bearing species ( $\text{N}_2$ ,  $\text{NH}_3$ ,  $\text{HCN}$  and other organics), as well as in the various nitrogen-bearing compounds found in Titan’s surface and atmosphere.

## 6. CONCLUSIONS

Using high signal-to-noise (13-1450) ALMA observations from 2019, we derived the first well-constrained isotopologue abundance ratios for  $\text{CH}_3\text{CN}$  in Titan’s atmosphere:  $68.9 \pm 4.2$  for  $\text{CH}_3\text{CN}/\text{CH}_3\text{C}^{15}\text{N}$ ,  $89.2 \pm 7.0$  for  $\text{CH}_3\text{CN}/^{13}\text{CH}_3\text{CN}$ , and  $91.2 \pm 6.0$  for  $\text{CH}_3\text{CN}/\text{CH}_3^{13}\text{CN}$ . These ratios represent disk-averaged values, but are most sensitive to gases in the altitude range 150-300 km, with a peak sensitivity around 230 km. We therefore show for the first time that  $^{15}\text{N}$  is strongly enhanced in  $\text{CH}_3\text{CN}$  compared to Titan’s main atmospheric nitrogen reservoir ( $\text{N}_2$ ). This can be explained as a result of photochemical isotopic fractionation initiated by isotope-selective photodissociation of  $\text{N}_2$  in the thermosphere. We find a consistent level of  $^{15}\text{N}$  enrichment within all Titan’s nitriles measured to date, which implies they likely formed from a common, isotopically fractionated reservoir of atmospheric nitrogen. Loss of atmospheric  $^{15}\text{N}$  due to isotopic fractionation into nitriles should therefore be considered as a potentially important isotope sink in future studies of the time-evolution of Titan’s atmospheric  $^{14}\text{N}/^{15}\text{N}$  ra-

tio, with implications for our understanding of the origins of Titan’s nitrogen reservoir. Comparison between our observed nitrogen isotopic ratio and the results from previous photochemical models shows better agreement with the Vuitton et al. (2019) model than the Dobrijevic & Loison (2018) that includes  $\text{N}_2$  dissociation by cosmic rays and mesospheric electrons, but there is still room for improvement, so the precise importance of these processes should be revisited in future modeling efforts. Future observations at higher signal-to-noise (by at least a factor of 5 for the minor isotopologue) will be required to investigate variability in the nitrile  $^{14}\text{N}/^{15}\text{N}$  ratios as a function of altitude.

## 7. ACKNOWLEDGMENTS

The National Radio Astronomy Observatory and Green Bank Observatory are facilities of the U.S. National Science Foundation operated under cooperative agreement by Associated Universities, Inc.

This paper makes use of the following ALMA data: ADS/JAO.ALMA#2019.1.00783.S. ALMA is a partnership of ESO (representing its member states), NSF (USA) and NINS (JAPAN), together with NRC (Canada), NSTC and ASIAA (Taiwan), and KASI (Republic of Korea), in cooperation with the Republic of Chile. The Joint ALMA Observatory is operated by ESO, AUI/NRAO, and NAOJ.

The work done by MAC, AET, and CAN was funded by NASA’s Solar System Observation (SSO) Program, this work was funded by the ALMA SOS program, and NAT was funded by STFC grant ST/Y000676/1.

## APPENDIX

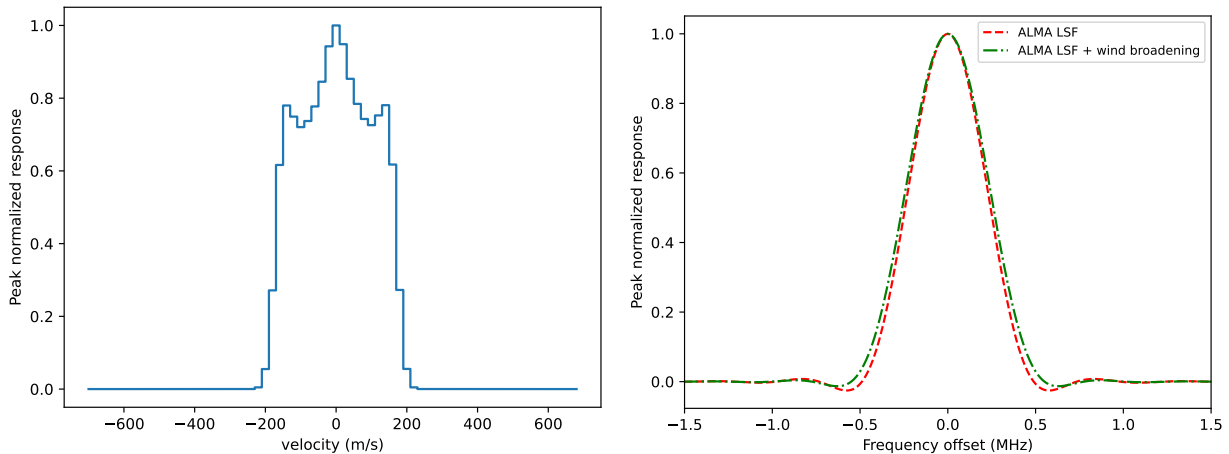
### A. $\text{CH}_3\text{CN}$ SPECTROSCOPIC PARAMETERS AND PARTITION FUNCTIONS

We used frequency predictions of acetonitrile (methyl cyanide;  $\text{CH}_3\text{CN}$ ) taken from the CDMS database (Müller et al. 2001) and noticed that the current CDMS predictions (Müller, H. S. P. et al. 2009) for the ground state were based on data with a significant missing window in experimental coverage around 257 GHz of current detections. The nearest experimental measurements were for the  $J=8-7$  transition near 147 GHz (Boucher et al. 1977) and then the  $J=18-17$  transition near 331 GHz (Cazzoli & Puzzarini 2006). For this reason we carried out an experimental double check of the prediction accuracy in this missing window, by measuring  $K=0$  to 9 transitions for  $J=14-13$  at 257 GHz and  $J=15-14$  at 275 GHz. Measurements were made at room temperature, and at around 1 mTorr sample pressure by using the broadband millimeter-wave (MMW) spectrometer in Warsaw (Medvedev et al. 2004). This verification turned out to be positive since CDMS predictions and currently measured frequencies for 20 different transitions were in agreement to a root mean square deviation of 16 kHz, which is well within the nominal uncertainty of the employed spectrometer.

Another issue that we faced in deriving the isotopic ratios was the need for a unified partition function for the parent species and its  $^{13}\text{C}$  isotopic variants. The values in the ground state entry in CDMS also accounted for the levels in the  $v_8=1$  excited vibrational state, while those for the  $^{13}\text{C}$  species did not. For this reason we re-evaluated the partition function for the ground state of the parent at the same conditions as for the isotopic species, namely without the  $v_8=1$  state, and without accounting for the nitrogen hyperfine structure, which is unresolved at the resolution of our data.

**Table 2.** Partition functions for CH<sub>3</sub>CN isotopologues as a function of temperature

T (K)	Q(CH <sub>3</sub> CN)	Q( <sup>13</sup> CH <sub>3</sub> CN)	Q(CH <sub>3</sub> <sup>13</sup> CN)	Q(CH <sub>3</sub> C <sup>15</sup> N)
300.0	10118.2635	10418.8811	10123.2613	10431.9556
225.0	6570.5621	6765.7543	6573.8080	6774.2565
150.0	3576.3518	3682.5661	3578.1185	3687.1996
75.00	1265.1853	1302.7260	1265.8098	1304.3662
37.50	449.0803	462.3803	449.3016	462.9618
18.75	164.3168	169.1645	164.3975	169.3765
9.375	64.0955	65.9716	64.1267	66.0537

**Figure 5.** Spectral line broadening profile based on the CH<sub>3</sub>CN wind field observed by [Cordiner et al. \(2020\)](#) (left), and final line spread function with wind induced broadening as well as the Hanning-smoothed sinc response of the ALMA correlator (right).

Omission of the CH<sub>3</sub>CN vibrationally excited state amounts to a 7% underestimation of the partition function. As a result of these improvements to the line intensities and partition functions, we found that the retrieved isotopic ratios decreased by 20% for the <sup>14</sup>N/<sup>15</sup>N ratio, 23% for the CH<sub>3</sub>CN/<sup>13</sup>CH<sub>3</sub>CN ratio and 27% for the CH<sub>3</sub>CN/CH<sub>3</sub><sup>13</sup>CN ratio.

## B. LINE SHAPE FUNCTION

In order to account for the potential effects of rotational broadening of the lines in the data, we generated a new instrumental line spread function for inclusion in NEMESIS. A rotationally broadened spectral profile was created using a modified version of the code published in [Cordiner et al. \(2020\)](#), including the impact of Titan’s winds on the CH<sub>3</sub>CN Doppler line profile based on the observed wind field in May 2017. We convolved the rotationally broadened profile with a line-shape function that mimics the ALMA correlator response, which is the Fourier transform of a (padded) Hann window, to get the new line spread function ([Hunter 2016](#)). Note the amount of padding used sets the frequency domain sampling and we set this to correspond to two channels, according to the standard setup of the ALMA correlator. Our observations were obtained at two different spectral resolutions (488 and 976 kHz), corresponding to a velocity FWHM of 568 and 1090 m s<sup>-1</sup> at 257.4461 and 267.5854 GHz, respectively. After the addition of wind broadening, the 488 kHz velocity FWHM increased to 604 m s<sup>-1</sup> (a difference of 36 m s<sup>-1</sup>), and the 976 kHz velocity FWHM increased to 1109 m s<sup>-1</sup> (a difference of 19 m s<sup>-1</sup>) so the line shape function (LSF) had a slight impact on the results.

## C. CONTINUOUS <sup>14</sup>N/<sup>15</sup>N PROFILE RETRIEVAL

To investigate the vertical behavior of the CH<sub>3</sub>CN/CH<sub>3</sub>C<sup>15</sup>N ratio, we used NEMESIS to perform a continuously variable abundance profile retrieval for CH<sub>3</sub>C<sup>15</sup>N, the result of which is shown in [Figure 6](#). The resulting <sup>14</sup>N/<sup>15</sup>N

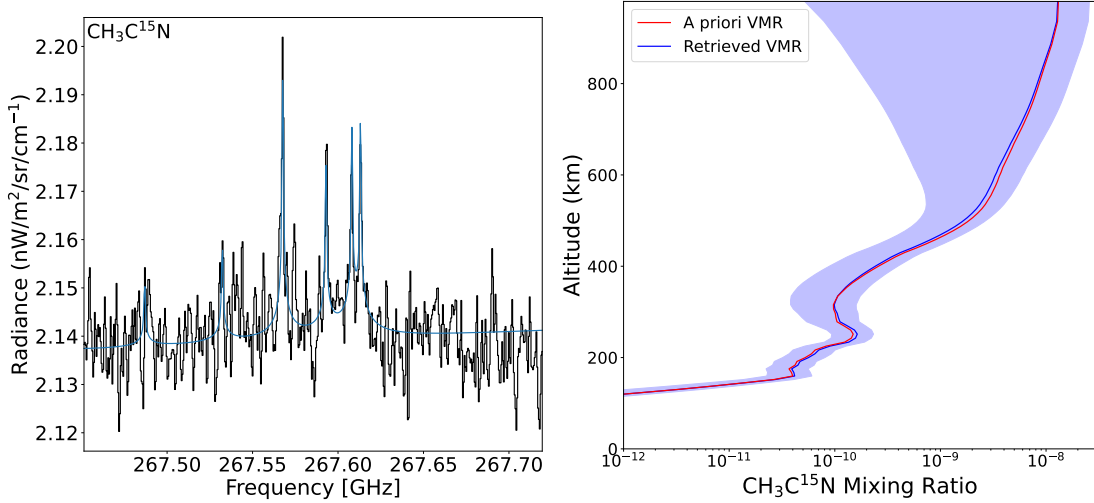


**Figure 6.** Continuously retrieved  $\text{CH}_3\text{C}^{15}\text{N}$  model fit (left) and VMR profile (right). As in 1(a) and 1(b), the data is in black and the model in blue and in the right panel the red line is the a priori profile, the blue line is the retrieved VMR profile and the shaded region is error on the retrieved VMR profile.

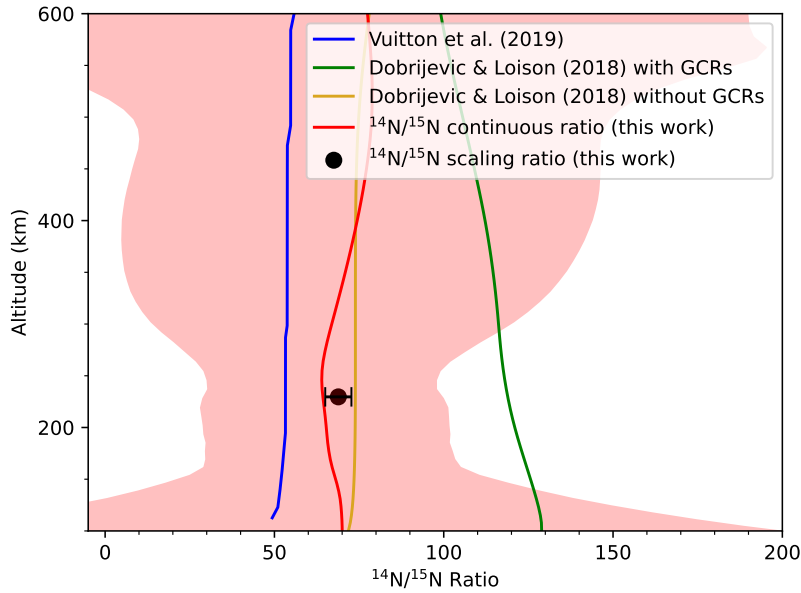


**Figure 7.** Derived continuous  $\text{CH}_3\text{CN}/\text{CH}_3\text{C}^{15}\text{N}$  isotopic ratio profile with error envelope (red; shaded red region) plotted with photochemical model profiles from Vuitton et al. (2019) (blue) and Dobrijevic & Loison (2018) (green and gold). The black point is our measured scaling factor for the  $\text{CH}_3\text{CN}/\text{CH}_3\text{C}^{15}\text{N}$  isotopic ratio from this work, plotted at the weighted mean emission altitude of 230 km (with its corresponding error bars).

ratio and error envelope is shown in Figure 7, where the errors represent the actual retrieval error, accounting for both the model and (lack of) a-priori errors. Since these errors are so large, there is no strong evidence for variability in the  $^{14}\text{N}/^{15}\text{N}$  ratio with altitude, based on our ALMA data.

As discussed in section 5, the two photochemical models make different assumptions about reaction pathways, including the weight given to interactions with magnetospheric electrons and cosmic rays, so further investigations of the  $^{14}\text{N}/^{15}\text{N}$  ratio as a function of altitude would be useful to help distinguish between the differing altitudinal dependencies as well as the impacts on the chemistry, as this will affect the abundance (and thus isotope) profiles differently at different altitudes.

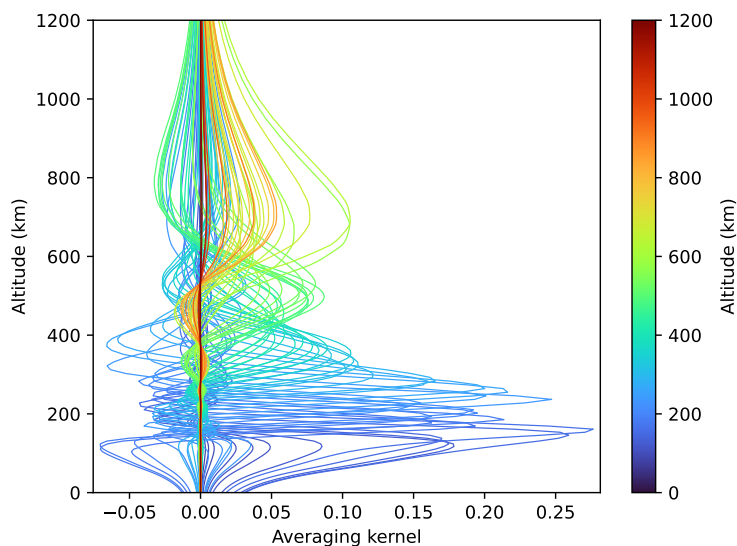


**Figure 8.** Averaging kernels for the  $\text{CH}_3\text{CN}$  major isotopologue, from our best-fitting NEMESIS model. The color bar shows the representative altitude applicable for each kernel. The altitudes with the largest values ( $\sim 150 - 300$  km) indicates the region of highest sensitivity of our model.

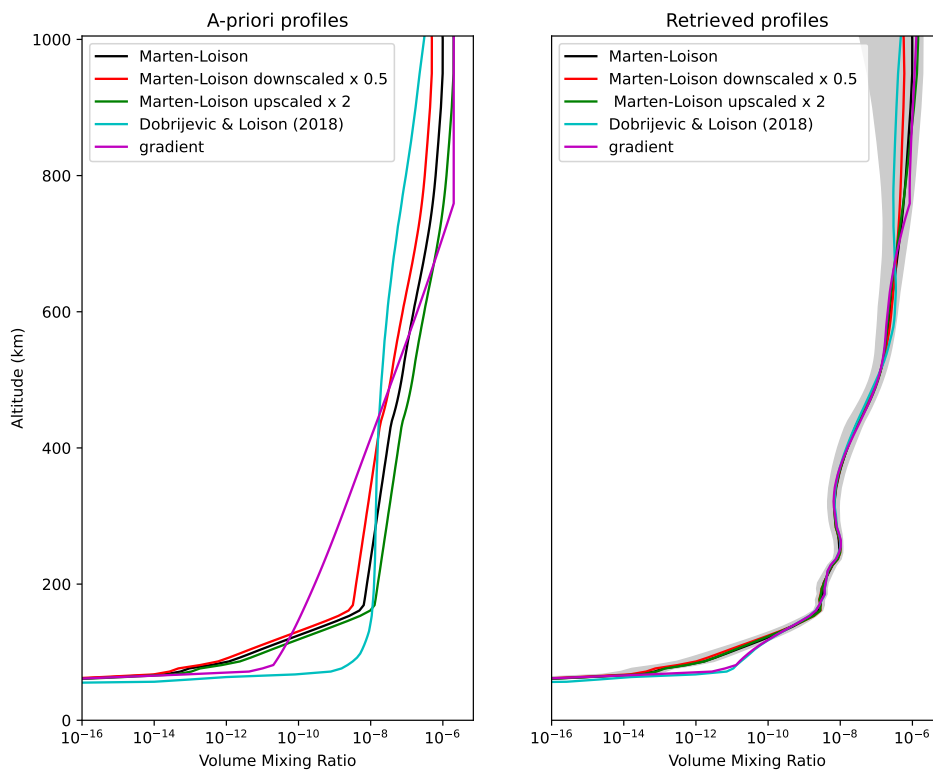


**Figure 9.** Plot of a-priori (left) and corresponding retrieved profiles (right) to investigate the sensitivity of the retrieved  $\text{CH}_3\text{CN}$  VMR to the shape of the a-priori. The retrieved  $\text{CH}_3\text{CN}$  VMR profile (black) is compared against retrievals using scaled versions of our default ‘Marten-Loison’ profile (green and red profiles), the [Dobrijevic & Loison \(2018\)](#) model profile (cyan) and a log-linear gradient profile (magenta) from [Thelen et al. \(2019\)](#). The gray shaded region in the right panel is the error on the default  $\text{CH}_3\text{CN}$  retrieved profile.

## D. AVERAGING KERNELS

The averaging kernels for an atmospheric abundance retrieval are the product of the gain matrix ( $G$ ) and Jacobian matrix ( $J$ ), and provide a representation of the correlation between the retrieved abundance of each atmospheric level with respect to the other levels. Averaging kernels for our best-fitting CH<sub>3</sub>CN NEMESIS model are shown in Figure 8. The averaging kernels can be used in tandem with the contribution functions to gain a better understanding of the origin of the spectral line emission and the sensitivity of the model. The altitudes with the largest kernel values (which also have the narrowest vertical envelopes), represent the region of the atmosphere to which our retrieved abundances are most sensitive, and with highest altitudinal resolution — *i.e.* in the range  $\sim 150$ – $300$  km. For more details on the formal definitions of  $G$ ,  $J$ , and the averaging kernel, see (Rodgers 1976).

## E. SENSITIVITY OF RETRIEVALS TO A PRIORI ASSUMPTIONS

Since our retrieved isotopic ratios are somewhat sensitive to the shape of the CH<sub>3</sub>CN major isotopologue VMR profile, it is important to investigate the degree to which that profile may depend on any a priori model assumptions. We therefore performed a set of CH<sub>3</sub>CN vertical abundance profile retrievals using different a priori profiles, including (1) scaled versions of our default a priori, (2) the CH<sub>3</sub>CN profile from Dobrijevic & Loison (2018), and (3) a gradient profile from Thelen et al. (2019). As shown in Figure 9, inside the altitudinal region to which our models are sensitive ( $\approx 125$ – $500$  km), the range where the peak-normalized emission contributions are greater than 1%, we find that the retrieved CH<sub>3</sub>CN abundance does not have any significant dependence on the choice of a priori.

## REFERENCES

- Altwegg, K., Balsiger, H., Hänni, N., et al. 2020, *Nature Astronomy*, 4, 533, doi: [10.1038/s41550-019-0991-9](https://doi.org/10.1038/s41550-019-0991-9)
- Balucani, N., Skouteris, D., Leonori, F., et al. 2012, *The Journal of Physical Chemistry A*, 116, 10467, doi: [10.1021/jp3072316](https://doi.org/10.1021/jp3072316)
- Borysow, A., & Frommhold, L. 1986a, *ApJ*, 303, 495, doi: [10.1086/164096](https://doi.org/10.1086/164096)
- . 1986b, *ApJ*, 304, 849, doi: [10.1086/164221](https://doi.org/10.1086/164221)
- . 1986c, *ApJ*, 311, 1043, doi: [10.1086/164841](https://doi.org/10.1086/164841)
- . 1987, *ApJ*, 318, 940, doi: [10.1086/165426](https://doi.org/10.1086/165426)
- Borysow, A., & Tang, C. 1993, *Icarus*, 105, 175, doi: <https://doi.org/10.1006/icar.1993.1117>
- Boucher, D., Burie, J., Demaison, J., et al. 1977, *Journal of Molecular Spectroscopy*, 64, 290, doi: [https://doi.org/10.1016/0022-2852\(77\)90267-3](https://doi.org/10.1016/0022-2852(77)90267-3)
- Bézard, B., Nixon, C. A., Kleiner, I., & Jennings, D. E. 2007, *Icarus*, 191, 397, doi: <https://doi.org/10.1016/j.icarus.2007.06.004>
- Cazzoli, G., & Puzzarini, C. 2006, *Journal of Molecular Spectroscopy*, 240, 153, doi: <https://doi.org/10.1016/j.jms.2006.09.013>
- Choukroun, M., Grasset, O., Tobie, G., & Sotin, C. 2010, *Icarus*, 205, 581, doi: <https://doi.org/10.1016/j.icarus.2009.08.011>
- Cordiner, M. A., Garcia-Berrios, E., Cosentino, R. G., et al. 2020, *The Astrophysical Journal Letters*, 904, L12, doi: [10.3847/2041-8213/abc688](https://doi.org/10.3847/2041-8213/abc688)
- Cordiner, M. A., Nixon, C. A., Charnley, S. B., et al. 2018, *The Astrophysical Journal Letters*, 859, L15, doi: [10.3847/2041-8213/aac38d](https://doi.org/10.3847/2041-8213/aac38d)
- Cordiner, M. A., Teanby, N. A., Nixon, C. A., et al. 2019, *The Astronomical Journal*, 158, 76, doi: [10.3847/1538-3881/ab2d20](https://doi.org/10.3847/1538-3881/ab2d20)
- Cordiner, M. A., Palmer, M. Y., Nixon, C. A., et al. 2015, *The Astrophysical Journal Letters*, 800, L14, doi: [10.1088/2041-8205/800/1/L14](https://doi.org/10.1088/2041-8205/800/1/L14)
- Courtin, R., Swinyard, B., Moreno, R., et al. 2011, *Astronomy & Astrophysics*, 536, L2
- Davies, A. G., Sotin, C., Choukroun, M., Matson, D. L., & Johnson, T. V. 2016, *Icarus*, 274, 23, doi: <https://doi.org/10.1016/j.icarus.2016.02.046>
- Dobrijevic, M., & Loison, J. 2018, *Icarus*, 307, 371, doi: <https://doi.org/10.1016/j.icarus.2017.10.027>
- Dudaryonok, A., Lavrentieva, N., & Buldyreva, J. 2015, *Icarus*, 250, 76, doi: <https://doi.org/10.1016/j.icarus.2014.11.020>
- Glein, C. R. 2015, *Icarus*, 250, 570, doi: <https://doi.org/10.1016/j.icarus.2015.01.001>
- Gurwell, M. A. 2004, *The Astrophysical Journal*, 616, L7, doi: [10.1086/423954](https://doi.org/10.1086/423954)
- Hidayat, T., Marten, A., Bézard, B., et al. 1997, *Icarus*, 126, 170
- Hunter, T. 2016, *Note on Spectral Response*, Tech. rep.
- Hörst, S. M. 2017, *Journal of Geophysical Research: Planets*, 122, 432, doi: <https://doi.org/10.1002/2016JE005240>



- Iino, T., Sagawa, H., & Tsukagoshi, T. 2020, *The Astrophysical Journal*, 890, 95, doi: [10.3847/1538-4357/ab66b0](https://doi.org/10.3847/1538-4357/ab66b0)
- Irwin, P., Teanby, N., de Kok, R., et al. 2008, *Journal of Quantitative Spectroscopy and Radiative Transfer*, 109, 1136, doi: <https://doi.org/10.1016/j.jqsrt.2007.11.006>
- Jacquinet-Husson, N., Scott, N., Chédin, A., et al. 2005, *Journal of Quantitative Spectroscopy and Radiative Transfer*, 95, 429, doi: <https://doi.org/10.1016/j.jqsrt.2004.12.004>
- Jennings, D. E., Nixon, C. A., Jolly, A., et al. 2008, *The Astrophysical Journal*, 681, L109, doi: [10.1086/590534](https://doi.org/10.1086/590534)
- Jolly, A., Fayt, A., Benilan, Y., et al. 2010, *ApJ*, 714, 852, doi: [10.1088/0004-637X/714/1/852](https://doi.org/10.1088/0004-637X/714/1/852)
- Kossacki, K. J., & Lorenz, R. D. 1996, *Planet. Space Sci.*, 44, 1029, doi: [10.1016/0032-0633\(96\)00022-0](https://doi.org/10.1016/0032-0633(96)00022-0)
- Kuiper, G. P. 1944, *ApJ*, 100, 378, doi: [10.1086/144679](https://doi.org/10.1086/144679)
- Lellouch, E., Gurwell, M. A., Moreno, R., et al. 2019, *An intense thermospheric jet on Titan.* <https://arxiv.org/abs/1903.12116>
- Liang, M.-C., Heays, A. N., Lewis, B. R., Gibson, S. T., & Yung, Y. L. 2007, *The Astrophysical Journal*, 664, L115, doi: [10.1086/520881](https://doi.org/10.1086/520881)
- Loison, J., Hébrard, E., Dobrijevic, M., et al. 2015, *Icarus*, 247, 218, doi: <https://doi.org/10.1016/j.icarus.2014.09.039>
- MacKenzie, S. M., Birch, S. P. D., Hörst, S., et al. 2021, *The Planetary Science Journal*, 2, 112, doi: [10.3847/PSJ/abf7c9](https://doi.org/10.3847/PSJ/abf7c9)
- Mandt, K. E., Mousis, O., Lunine, J., & Gautier, D. 2014, *The Astrophysical Journal Letters*, 788, L24, doi: [10.1088/2041-8205/788/2/L24](https://doi.org/10.1088/2041-8205/788/2/L24)
- Mandt, K. E., Waite, J. H., Teolis, B., et al. 2012, *ApJ*, 749, 160, doi: [10.1088/0004-637X/749/2/160](https://doi.org/10.1088/0004-637X/749/2/160)
- Marten, A., Hidayat, T., Biraud, Y., & Moreno, R. 2002, *Icarus*, 158, 532, doi: <https://doi.org/10.1006/icar.2002.6897>
- Medvedev, I., Winnewisser, M., De Lucia, F. C., et al. 2004, *Journal of Molecular Spectroscopy*, 228, 314, doi: <https://doi.org/10.1016/j.jms.2004.06.011>
- Molter, E. M., Nixon, C. A., Cordiner, M. A., et al. 2016, *The Astronomical Journal*, 152, 42, doi: [10.3847/0004-6256/152/2/42](https://doi.org/10.3847/0004-6256/152/2/42)
- Müller, H. S. P., Thorwirth, S., Roth, D. A., & Winnewisser, G. 2001, *A&A*, 370, L49, doi: [10.1051/0004-6361:20010367](https://doi.org/10.1051/0004-6361:20010367)
- Müller, H. S. P., Drouin, B. J., & Pearson, J. C. 2009, *A&A*, 506, 1487, doi: [10.1051/0004-6361/200912932](https://doi.org/10.1051/0004-6361/200912932)
- Niemann, H. B., Atreya, S. K., Demick, J. E., et al. 2010, *Journal of Geophysical Research: Planets*, 115, doi: <https://doi.org/10.1029/2010JE003659>
- Nixon, C., Achterberg, R., Vinatier, S., et al. 2008a, *Icarus*, 195, 778, doi: <https://doi.org/10.1016/j.icarus.2008.01.012>
- Nixon, C., Lorenz, R., Achterberg, R., et al. 2018, *Planetary and Space Science*, 155, 50, doi: <https://doi.org/10.1016/j.pss.2018.02.009>
- Nixon, C. A. 2024, *ACS Earth and Space Chemistry*, 8, 406–456, doi: [10.1021/acsearthspacechem.2c00041](https://doi.org/10.1021/acsearthspacechem.2c00041)
- Nixon, C. A., Jennings, D. E., Bézard, B., et al. 2008b, *The Astrophysical Journal*, 681, L101, doi: [10.1086/590553](https://doi.org/10.1086/590553)
- Nixon, C. A., Temelso, B., Vinatier, S., et al. 2012, *The Astrophysical Journal*, 749, 159, doi: [10.1088/0004-637X/749/2/159](https://doi.org/10.1088/0004-637X/749/2/159)
- Nomura, H., Furuya, K., Cordiner, M., et al. 2022. <https://arxiv.org/abs/2203.10863>
- Oro, J., Miller, S. L., & Lazcano, A. 1990, *Annual Review of Earth and Planetary Sciences*, 18, 317, doi: <https://doi.org/10.1146/annurev.earth.18.050190.001533>
- Palmer, M. Y., Cordiner, M. A., Nixon, C. A., et al. 2017, *Science Advances*, 3, e1700022, doi: [10.1126/sciadv.1700022](https://doi.org/10.1126/sciadv.1700022)
- Rengel, M., Sagawa, H., & Hartogh, P. 2011, *NEW SUB-MILLIMETER HETERODYNE OBSERVATIONS OF CO AND HCN IN TITAN'S ATMOSPHERE WITH THE APEX SWEDISH HETERODYNE FACILITY INSTRUMENT* (World Scientific Publishing Co. Pte. Ltd.), 173–185, doi: [10.1142/9789814355377\\_0013](https://doi.org/10.1142/9789814355377_0013)
- Rengel, M., Shulyak, D., Hartogh, P., et al. 2022, *A&A*, 658, A88, doi: [10.1051/0004-6361/202141422](https://doi.org/10.1051/0004-6361/202141422)
- Rengel, M., Sagawa, H., Hartogh, P., et al. 2014, *A&A*, 561, A4, doi: [10.1051/0004-6361/201321945](https://doi.org/10.1051/0004-6361/201321945)
- Rodgers, C. D. 1976, *Reviews of Geophysics*, 14, 609, doi: <https://doi.org/10.1029/RG014i004p00609>
- Serigano, J., Nixon, C. A., Cordiner, M. A., et al. 2016, *The Astrophysical Journal Letters*, 821, L8, doi: [10.3847/2041-8205/821/1/L8](https://doi.org/10.3847/2041-8205/821/1/L8)
- Teanby, N., Irwin, P., Nixon, C., et al. 2013, *Planetary and Space Science*, 75, 136, doi: <https://doi.org/10.1016/j.pss.2012.11.008>
- Teanby, N. A., Sylvestre, M., Sharkey, J., et al. 2019, *Geophysical Research Letters*, 46, 3079, doi: <https://doi.org/10.1029/2018GL081401>
- Teanby, N. A., de Kok, R., Irwin, P. G. J., et al. 2008, *Journal of Geophysical Research: Planets*, 113, doi: <https://doi.org/10.1029/2008JE003218>

- Teanby, N. A., Bézard, B., Vinatier, S., et al. 2017, *Nature Communications*, 8, 1586,  
doi: [10.1038/s41467-017-01839-z](https://doi.org/10.1038/s41467-017-01839-z)
- Thelen, A. E., Nixon, C., Chanover, N., et al. 2019, *Icarus*, 319, 417,  
doi: <https://doi.org/10.1016/j.icarus.2018.09.023>
- Thelen, A. E., Cordiner, M. A., Nixon, C. A., et al. 2020, *The Astrophysical Journal Letters*, 903, L22,  
doi: [10.3847/2041-8213/abc1e1](https://doi.org/10.3847/2041-8213/abc1e1)
- Thelen, A. E., Nixon, C. A., Cordiner, M. A., et al. 2024, *The Planetary Science Journal*, 5, 125,  
doi: [10.3847/PSJ/ad47bd](https://doi.org/10.3847/PSJ/ad47bd)
- Tobie, G., Lunine, J. I., & Sotin, C. 2006, *Nature*, 440, 61,  
doi: [10.1038/nature04497](https://doi.org/10.1038/nature04497)
- Vinatier, S., Bézard, B., & Nixon, C. A. 2007, *Icarus*, 191, 712, doi: [10.1016/j.icarus.2007.06.001](https://doi.org/10.1016/j.icarus.2007.06.001)
- Vuitton, V., Yelle, R., Klippenstein, S., Hörst, S., & Lavvas, P. 2019, *Icarus*, 324, 120,  
doi: <https://doi.org/10.1016/j.icarus.2018.06.013>
- Willacy, K., Allen, M., & Yung, Y. 2016, *The Astrophysical Journal*, 829, 79, doi: [10.3847/0004-637x/829/2/79](https://doi.org/10.3847/0004-637x/829/2/79)
- Wilson, E. H., & Atreya, S. K. 2004, *Journal of Geophysical Research: Planets*, 109,  
doi: <https://doi.org/10.1029/2003JE002181>